Applied Physics Letters

# Atomic-scale imaging of interfacial polarization in cuprate-titanate heterostructures

Cite as: Appl. Phys. Lett. **116**, 251603 (2020); https://doi.org/10.1063/5.0011081
Submitted: 17 April 2020 . Accepted: 07 June 2020 . Published Online: 23 June 2020

Shao-Bo Mi, Tian Yao, Shao-Dong Cheng, Micheal I. Faley, Ulrich Poppe, Lu Lu, Dawei Wang, and Chun-Lin Jia



Applied Physics Letters ARTICLE scitation.org/journal/apl

# Atomic-scale imaging of interfacial polarization in cuprate-titanate heterostructures

Cite as: Appl. Phys. Lett. **116**, 251603 (2020); doi: 10.1063/5.0011081
Submitted: 17 April 2020 · Accepted: 7 June 2020 ·
Published Online: 23 June 2020



Shao-Bo Mi,[1,a] Tian Yao,[1] Shao-Dong Cheng,[1,2] Micheal I. Faley,[3] Ulrich Poppe,[3] Lu Lu,[1,2] Dawei Wang,[1,2] and Chun-Lin Jia[1,2,3]

## AFFILIATIONS

[1]State Key Laboratory for Mechanical Behavior of Materials, Xi'an Jiaotong University, Xi'an 710049, China
[2]School of Microelectronics, Xi'an Jiaotong University, Xi'an 710049, China
[3]Ernst Ruska Centre for Microscopy and Spectroscopy with Electrons and Peter Grünberg Institute, Forschungszentrum Jülich, D-52425 Jülich, Germany

[a)]Author to whom correspondence should be addressed: shaobo.mi@xjtu.edu.cn

## ABSTRACT

The interfaces in oxide heterostructures that bring novel physical phenomena and functionalities have attracted great attention in fundamental research and device applications. For uncovering structure–property relationships of oxide heterostructures, direct evidence of the atomic-scale structure of heterointerfaces is highly desired. Here, we report on studying the structure of interfaces between $YBa_2Cu_3O_{7-\delta}$ thin films and $SrTiO_3$ substrates by means of aberration-corrected ultrahigh-resolution electron microscopy. Employing advanced imaging and spectroscopic techniques, shifts of atoms at the interface away from the regular lattice sites are measured, leading to the interfacial polarity. The local polarization induced by the atomic shifts directs toward the cuprate films and is estimated to be about 36.1 $\mu C/cm^2$. The observed interfacial polar layer is understood by the special atomic configuration across the interface, which could modulate the electrical properties in superconducting devices that are based on the ferroelectric/superconductor heterosystems.



Heterostructures of perovskite-based oxide materials have attracted extensive attention from both fundamental research and technological applications because of their variety of fascinating physical properties.[1,2] It has been demonstrated that interfaces in the designed heterostructures have striking properties, which do not exist in either of the constituent bulk materials, e.g., 2D electron gas at the $LaAlO_3/SrTiO_3$ (LAO/STO) interface.[3,4] In addition, the functionalities of the perovskite-based oxide epitaxial layers can be modulated by the field effect arising from the adjacent layers or/and the interface coupling in heterostructures (e.g., proximity effects in superconductor–ferromagnet heterostructures).[5–7] Among the perovskite-based heterostructures, strongly electron-correlated materials are of essential importance due to their applications in superconducting field-effect devices, e.g., high-temperature superconducting (HTS) ultrathin films grown on insulating STO substrates.[8–10] In these heterostructures, the critical temperature ($T_c$) and phase transitions of the HTS cuprate films can be tuned by an external electric field without involving chemical and crystalline modulation of the materials. Also, it was reported that the $T_c$ of the ultrathin HTS films can be shifted by the charge carriers, which are injected by the dielectric gate polarization under an applied electric field and thus leading to a suppression of superconductivity in the ultrathin HTS films.[11–14]

The Thomas–Fermi screening length ($\lambda_{TF}$) of $YBa_2Cu_3O_{7-\delta}$ (YBCO) is on the order of ~1 nm.[15] Therefore, the interface coupling between the dielectric gate and the YBCO films has important effect on shifting $T_c$ of the ultrathin YBCO films. In particular, the interfacial polarity of the heterostructures has been expected to change the doping level and thus to affect the superconductivity of the unit-cell-thick HTS cuprate films.[16] Although the experimental and theoretical investigations have been performed on studying HTS heterostructures,[9,10,17–19] the interfacial atomic arrangement of superconducting/insulating heterostructures, including reconstructions, relaxations, interatomic mixing, and distortions, is necessary to be clarified for a deep insight into the mechanisms behind the experimentally measured interface-related properties. In this work, we provide the atomic-scale interface structure of YBCO/STO(001) obtained by using high-resolution imaging and spectroscopic techniques of aberration-corrected transmission electron microscopy (TEM) and scanning transmission electron microscopy (STEM).

The YBCO superconducting films were prepared on $TiO_2$-terminated STO(001) single crystal substrates (obtained as described in Ref. 20) using polycrystalline YBCO targets by the high-oxygen-pressure sputtering technique. During deposition, the substrates were positioned freely on the heater, which leads to a substrate temperature of about 850 °C. The YBCO films were deposited in an oxygen atmosphere (99.999% purity) at a pressure of 3 mbar. Cross-sectional specimens for TEM observations were prepared by a standard procedure, including grinding, dimpling, and polishing. The final thinning was performed by Ar ion milling on a sample stage cooled by liquid nitrogen. Atomic-scale high-angle annular dark-field (HAADF) and annular bright-field (ABF) STEM images were recorded on a JEOL JEM-ARM200F microscope with a probe aberration corrector and an Oxford X-MaxN 100TLE spectrometer, operated at 200 kV. High-resolution negative $C_S$ imaging (NCSI)[21] was performed on an FEI Titan 80–300 microscope with an aberration corrector for the objective lens, operated at 300 kV. In the high-resolution TEM (HRTEM) imaging mode, a small negative $C_S$ value of $-13$ $\mu$m was adjusted for the objective lens to meet the NCSI conditions.[22] Structural modeling and image simulations were carried out using the CrystalKitX-MacTempasX software package.[23] The position of image intensity peaks in the NCSI image was measured by using the iMtools software package.[24]

Figure 1(a) shows a typical HAADF-STEM image of the YBCO/STO interface recorded along the crystallographic [010] STO zone axis. By averaging the intensity over 12 unit cells parallel to the interface from the experimental HAADF image displayed in Fig. 1(a), a noise-reduced HAADF-STEM image can be obtained, as shown in Fig. 1(b). The chemistry across the heterointerface can be qualitatively estimated under the HAADF-STEM imaging conditions. The intensity of the peaks in the YBCO film layer decreases from the Ba columns giving the brightest contrast via the Y and CuO to $CuO_{1-\delta}$ columns. In the STO substrate, the brightest peaks are for the Sr atom columns and the less bright are for the Ti-O columns. In contrast, the oxygen columns, due to the low nuclear charge, do not give rise to enough contrast to be detected. According to the image contrast variation, BaO and SrO atomic planes in the system of YBCO and STO can be easily identified at the film–substrate interface, indicated by a yellow and a green horizontal arrow, respectively. At the heterointerface, an atomic plane between the interfacial BaO and SrO atomic planes marked by a red horizontal arrow is either a $TiO_2$ plane belonging to STO or a $CuO_{1-\delta}$ plane of YBCO according to the (001) stacking sequence of the two compounds.

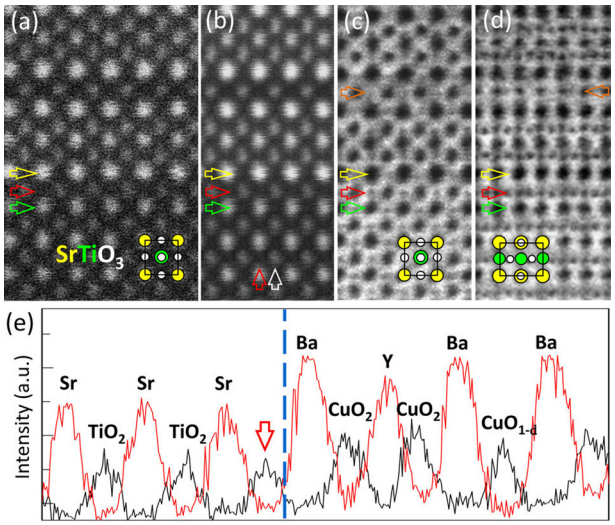


**FIG. 1.** (a) High-resolution HAADF-STEM image of the YBCO/STO (001) interface taken along the [010] STO zone axis. (b) The image obtained by averaging the experimental image (a) parallel to the interface. (c) and (d) ABF-STEM image of the YBCO/STO(001) interface, viewed along the [010] and [110] STO zone axes, respectively. Interfacial BaO and SrO planes are indicated by a yellow and a green arrow, respectively. $CuO_{1-\delta}$ plane in YBCO is indicated by an orange arrow. The interfacial layer is indicated by a red arrow. (e) Intensity profile measured along the plane indicated by a red and a white arrow in the (b). A vertical red arrow marks the intensity peak of the atomic column in the interfacial plane denoted by the horizontal red arrow in (b).

Additionally, ABF-STEM images of the YBCO/STO interface were recorded along both the [010] and [110] zone axes of STO, as shown in Figs. 1(c) and 1(d), respectively. Both oxygen and cation columns are visible under the ABF-STEM imaging conditions,[25] which allow us to investigate the arrangement of oxygen atoms for distinguishing the difference between the $TiO_2$ and the $CuO_{1-\delta}$ planes. From the ABF-STEM images, the intensity at the oxygen positions in the interfacial plane (red arrows) is evident and comparable with that in the $TiO_2$ plane. In comparison, the intensity at the similar position of the $CuO_{1-\delta}$ planes (orange arrows) is hardly visible. Figure 1(e) shows the intensity profiles of the peak at atomic columns. The intensity profiles were obtained by scanning the atomic planes indicated by vertical arrows in Fig. 1(b). The corresponding intensity at the atomic column indicated by a red vertical arrow in Fig. 1(e) is evidently lower than that of the columns in the $CuO_{1-\delta}$ plane, but comparable with that of the columns in the $TiO_2$ atomic plane.

To obtain further evidence for the nature of the interfacial atomic plane, the atomic-resolved energy-dispersive X-ray spectroscopy (EDS) mapping has been applied to the element analysis at the

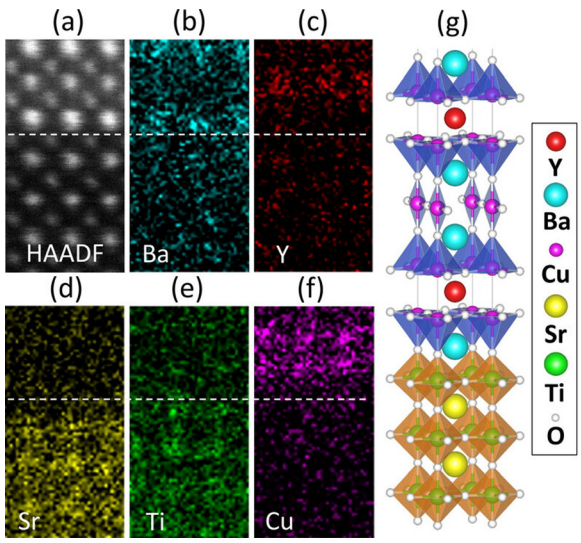


**FIG. 2.** (a)–(f) A magnified HAADF-STEM image of the YBCO/STO (001) interface and the corresponding EDS map of Ba, Y, Sr, Ti, and Cu, respectively, viewed along the [010] STO zone axis. White broken-line denotes the interface.

interface. Figures 2(a)–2(f) show a magnified HAADF-STEM image and the corresponding EDS map of elements Ba, Y, Sr, Ti, and Cu of the YBCO/STO interface, respectively, viewed along the [010] STO zone axis. A white broken-line denotes the interface. Figures 2(b) and 2(e) indicate that the YBCO film and the STO substrate terminate at the BaO and $TiO_2$ atomic planes at the interface, respectively. No diffusion of Cu into the Ti sublattice is discerned in Figures 2(e) and 2(f). Accordingly, the stacking sequence of the atomic plane across the YBCO/STO interface is determined as bulk–SrO–$TiO_2$–BaO–$CuO_2$–Y–$CuO_2$–BaO–CuO–BaO–bulk, as schematically displayed in Fig. 2(g), which maintains the continuity of the perovskite structure at the interface. This stacking sequence has the strongest interfacial adhesion according to the first-principles calculations among 48 types of the interface structure of the YBCO/STO heterojunction.[17]

Figure 3(a) shows an atomic-resolution NCSI image of the YBCO/STO interface recorded along the crystallographic [110] direction of STO. In Fig. 3(a), all atomic columns along the projected direction appear bright under a dark background.[21,22] Interestingly, the oxygen-atom positions in the interfacial $TiO_2$ layer apparently shift downwards with respect to the Ti positions, which is essentially different from that of the other $TiO_2$ atomic planes in the STO bulk, as shown in the magnified image of the YBCO/STO interface in Fig. 3(b). As a comparison, a calculated image is shown as an inset in Fig. 3(b), which has the best fit to the experimental image. The best-fitting simulated image was obtained by an iterative procedure for comparison with the experimental image.[26] Based on the image simulation image artifacts, e.g., the image intensity peaks deviating from the atom positions induced by residual lens aberrations and a small crystal tilt were evaluated and removed from the data of atom positions.

The unit cells of STO and YBCO are indexed by $i$ (= −7–4) for quantitative analysis in Fig. 3(a), and the position of the image intensity peaks in the NCSI image was determined by fitting a two-dimensional Gaussian function to the intensity distribution around the intensity peaks.[24,26] Figure 4(a) shows the value of the $c$-lattice parameter across the interface for the indexed unit cells in Fig. 3(a), measured from the SrO to SrO atomic plane in STO and from the Y to Y atomic plane in YBCO. The lattice parameters across the interface were calculated on the basis of the determined positions of intensity peaks, and the measured value has been calibrated using the lattice parameter of STO (0.3905 nm). The value of the $c$-lattice parameter of the YBCO films is 1.186 ± 0.003 nm, which is slightly larger than the bulk value (1.1708 nm[27]). At the interface, the interfacial SrO atomic plane slightly shifts toward the interface, resulting in 0.392 nm for the $c$-lattice parameter of the unit cell $i = -2$ in the STO substrate close to the interface. At the interface, the spacing between the SrO and BaO atomic planes (unit cell $i = -1$) was measured to be 0.414 nm, which is much larger than the lattice parameter of the bulk $SrTiO_3$ and $BaTiO_3$.[28] It is known that the YBCO HTS phase has an orthorhombic ($a = 0.3827$ nm, $b = 0.3877$ nm, and $c = 1.1708$ nm[27]) structure at room temperature. For the epitaxial $c$-orientated film, the YBCO lattice is constrained by the STO substrate lattice, resulting in a tensile strain in the film. Our results indicate that the interface coupling

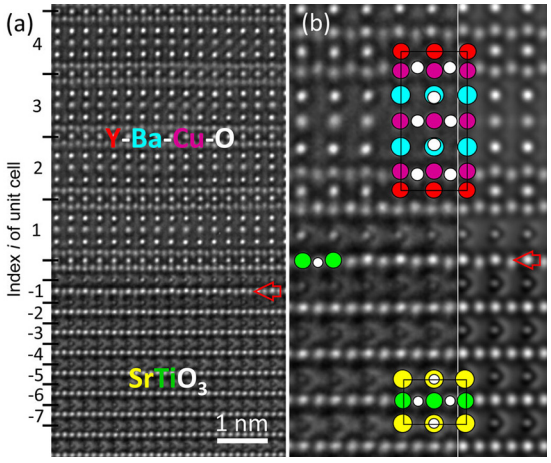


**FIG. 3.** (a) Atomic-resolution NSCI image of the YBCO/STO (001) interface recorded along the crystallographic [110] direction. (b) A magnified NCSI image of the YBCO/STO (001) interface showing the apparent buckling of the interfacial $TiO_2$ plane along the out-of-plane direction. The interfacial $TiO_2$ plane is indicated by a horizontal red arrow. The inset shows the best-fitting simulated image obtained by performing an iterative procedure for comparison between simulated and experimental images. The simulation parameters: sample thickness (STO) ($t$) = 6.9 nm, defocus ($\Delta f$) = +4.2 nm, twofold astigmatism ($A_2$) = 2 nm, threefold astigmatism ($A_3$) = 20 nm, axis coma ($B_2$) = 20 nm, a crystal tilt of 1.5 mrad, and a vibration of 0.03 nm.

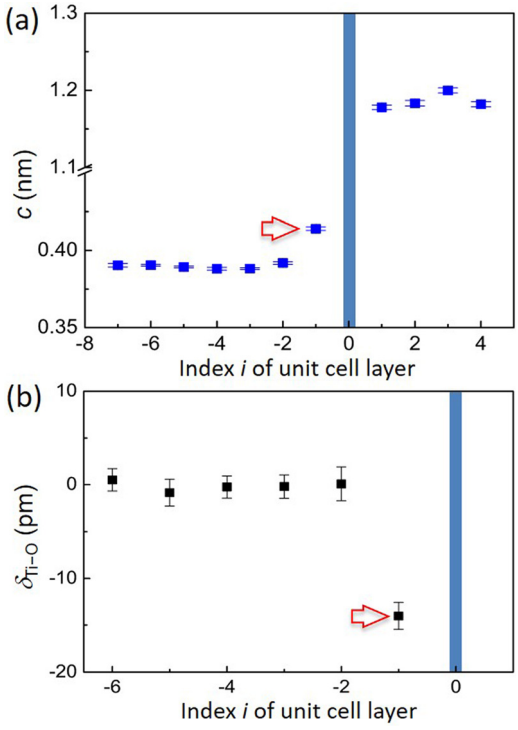


**FIG. 4.** (a) The $c$-lattice parameter of STO and YBCO across the interface measured from SrO to SrO atom positions in STO and from Y to Y in YBCO, respectively. A red horizontal arrow indicates the measured value of the distance from the Sr to Ba atom position for the interfacial unit ($i = -1$). (b) The relative displacement ($\delta_{Ti\text{-}O}$) between O and Ti in $TiO_2$ planes for the unit cell layers ($i = -6$ to $-1$) of STO. A red horizontal arrow shows the off-center displacement of oxygen atoms in the interfacial $TiO_2$ plane ($i = -1$). Note that the unit cell layers of STO and YBCO displayed in Fig. 3(a) were indexed with $i = -7$–4 for quantitative analysis of lattice parameters and atom displacements.

between YBCO and STO slightly affects the out-of-plane lattice parameter of the unit cell of STO and YBCO at the interface.

Figure 4(b) displays the [001] off-center displacement values ($\delta_{Ti-O}$) of the oxygen atoms relative to the neighboring Ti atom positions in the interface region of the STO substrate. For the interfacial unit cell ($i = -1$), the off-center displacement of oxygen atoms in the $TiO_2$ plane is about 14 picometers, while in other STO unit cells, the displacement ($\delta_{Ti-O}$) is essentially zero. The negative value of $\delta_{Ti-O}$ means that the oxygen atoms have a downward displacement with respect to the Ti atoms. The statistical measurement errors displayed in Fig. 4 are calculated from the regression procedure for the image intensity peak in Fig. 3(a). The position of a single atomic column is measured within a $2\sigma$ error radius (2 pm), demanding a statistical confidence of 95%. It should be mentioned that both ABF-STEM imaging and NCSI imaging can, in principle, be applied to measure the subtle atomic displacements at the YBCO/STO interface.

At the YBCO/STO interface, in the interfacial unit ($i = -1$), both the Ti and O atoms show shifts, and the mean value of relative displacement between O and Ti is about 14 picometers, leading to the formation of the Ti−O buckling along the interface. In displacive ferroelectric compounds, the spontaneous polarization ($P_S$) can be related to the displacement ($\Delta Z$) of the cation column from the center of the oxygen octahedron by an empirical formula, $P_s = \kappa \Delta Z$, where $\kappa$ is a constant with unit ($\mu C/cm^2$) $Å^{-1}$ and about 258 ± 9 ($\mu C/cm^2$) $Å^{-1}$ for displacive ferroelectric crystals for calculating $P_S$.[28] Using this formula, the calculated spontaneous polarization ($P_S$) for the interfacial unit cell ($i = -1$) is about 36.1 $\mu C/cm^2$ based on the relative displacement ($\Delta Z = 0.014$ nm) between Ti and O, which is slightly larger than that in the bulk $BaTiO_3$ (0.0132 nm).[28]

In the interfacial $TiO_2$ layer, the oxygen atoms with respect to the Ti atoms always shift toward the SrO atomic plane, which results in the spontaneous polarization of the single unit cell layer toward the BaO atomic plane of YBCO. Within a simple ionic model of STO and YBCO, the valences of ions are +2 for Sr, +4 for Ti, −2 for O, +3 for Y, +2 for Ba, and about +2.3 for Cu in nearly fully oxygenated YBCO.[29,30] The atomic planes of BaO, $TiO_2$, and SrO are electrically neutral. As a result, the observed stacking sequence of atomic planes across the YBCO/STO interface leads to a local charge imbalance from the negatively charged $CuO_2$ layer next to the interface block, which can, in principle, be compensated by an interface dipole layer of the $TiO_2$ layer with the observed spontaneous polarization. The observed buckling of the $CuO_2$ plane above and below the $Y^{3+}$ plane in the YBCO is noted, where the negatively charged oxygen ions are attracted to the positively charged $Y^{3+}$ layer. In the interfacial buckling $TiO_2$ layer ($i = -1$), the positive $Ti^{+4}$ atoms are Coulomb-attracted to the negatively charged interfacial $CuO_2$ plane (charge ca. −1.7) and the negatively charged $O^{2-}$ ions are repelled from the negatively charged interfacial $CuO_2$ plane.

In the heterosystems containing ferroelectric $Pb(Zr,Ti)O_3$ film and HTS cuprates, the Ti−O displacement at the interface substantially affect the inner carrier density and the properties of HTS films (e.g., the suppression of $T_c$ for highly doped HTS cuprate films and the difference in the electric field effect on under-doped and over-doped HTS).[5,12,13] Considering the occurrence of spontaneous polarization at the YBCO/STO interface, the effect of the polarization-induced electric field on the properties of HTS films is, in principle, identical to that in the ferroelectric/superconductor systems. In addition, our experimental observations confirm the film growth mode of YBCO on STO with an incomplete cuprate unit cell on the STO substrates, resulting in the effective interface doping by the hole carriers concentrated in the $CuO_2$ atomic planes.[16,31,32] Therefore, apart from the effect of interface disorder resulting from the STO steps,[10,19] the surface states arising from the spontaneous polarization observed at the YBCO/STO(001) interface could substantially affect the superconducting properties of the YBCO films, e.g., the critical current density and $T_c$.[9,10]

In summary, we demonstrate experimental evidence that the spontaneous polarization caused by the interface coupling occurs at the YBCO/STO(001) interface. The electrostatic modulation of superconductivity in ultrathin YBCO films can be expected, which results from the polarization charge transfer across the interface. Certainly, to entirely understand the effects of interface coupling in the heterostructures on the properties of the field-effect device, more experimental and theoretical studies based on the present results are required. Nevertheless, it is believed that tuning $T_c$ in HTS films can be achieved by the carefully controlled interface structure using advanced synthesis methods with atomic-scale precision.

This work was supported by the National Natural Science Foundation of China (Nos. 51071156, 51471169, and 51390472).

## DATA AVAILABILITY

The data that support the findings of this work are available from the corresponding author upon reasonable request.

## REFERENCES

[1]X. Wei, Y. Yang, L. McGilly, L. Feigl, R. Dunin-Borkowski, C. L. Jia, L. Bellaiche, and N. Setter, Phys. Rev. B **98**, 020102 (2018).
[2]J. F. Scott and C. A. P. De Araujo, Science **246**, 1400 (1989).
[3]A. Ohtomo and H. Y. Hwang, Nature **427**, 423 (2004).
[4]S. Thiel, G. Hammerl, A. Schmehl, C. W. Schneider, and J. Mannhart, Science **313**, 1942 (2006).
[5]C. H. Ahn, S. Gariglio, P. Paruch, T. Tybell, L. Antognazza, and J.-M. Triscone, Science **284**, 1152 (1999).
[6]S. Yunoki, A. Moreo, E. Dagotto, S. Okamoto, S. S. Kancharla, and A. Fujimori, Phys. Rev. B **76**, 064532 (2007).
[7]A. I. Buzdin, Rev. Mod. Phys. **77**, 935 (2005).
[8]A. Walkenhorst, C. Doughty, X. Xi, S. Mao, Q. Li, T. Venkatesan, and R. Ramesh, Appl. Phys. Lett. **60**, 1744 (1992).
[9]J. Mannhart, D. G. Schlom, J. G. Bednorz, and K. A. Müller, Phys. Rev. Lett. **67**, 2099 (1991).
[10]X. Xi, C. Doughty, A. Walkenhorst, C. Kwon, Q. Li, and T. Venkatesan, Phys. Rev. Lett. **68**, 1240 (1992).
[11]S. Sakai, Phys. Rev. B **47**, 9042 (1993).
[12]N. Pavlenko, Phys. Rev. B **70**, 094519 (2004).
[13]A. Cassinese, G. M. De Luca, A. Prigiobbo, M. Salluzzo, and R. Vaglio, Appl. Phys. Lett. **84**, 3933 (2004).
[14]N. Pavlenko and F. Schwabl, Appl. Phys. Lett. **86**, 012507 (2005).
[15]M. Rasolt, T. Edis, and Z. Tešanović, Phys. Rev. Lett. **66**, 2927 (1991).
[16]N. Pavlenko, I. Elfimov, T. Kopp, and G. A. Sawatzky, Phys. Rev. B **75**, 140512(R) (2007).
[17]Z. C. Wang, S. Tsukimoto, M. Saito, and Y. Ikuhara, J. Appl. Phys. **106**, 093714 (2009).
[18]R. Ramesh, A. Inam, D. M. Hwang, T. S. Ravi, T. Sands, X. X. Xi, X. D. Wu, Q. Li, T. Venkatesan, and R. Kilaas, J. Mater. Res. **6**, 2264 (1991).
[19]J. Garcia-Barriocanal, A. M. Perez-Munoz, Z. Sefrioui, D. Arias, M. Varela, C. Leon, S. J. Pennycook, and J. Santamaria, Phys. Rev. B **87**, 245105 (2013).
[20]G. Koster, B. L. Kropman, G. J. H. M. Rojnders, D. H. A. Blank, and H. Rogalla, Appl. Phys. Lett. **73**, 2920 (1998).

[21]C. L. Jia, M. Lentzen, and K. Urban, Science **299**, 870 (2003).
[22]C. L. Jia, M. Lentzen, and K. Urban, Microsc. Microanal. **10**, 174 (2004).
[23]M. A. O'Keefe and R. Kilaas, Scan Microsc. Suppl. **2**, 225 (1988).
[24]L. Houben, A. Thust, and K. Urban, Ultramicroscopy **106**, 200 (2006).
[25]S. D. Findlay, N. Shibata, H. Sawada, E. Okunishi, Y. Kondo, T. Yamamoto, and Y. Ikuhara, Appl. Phys. Lett. **95**, 191913 (2009).
[26]C. L. Jia, S. B. Mi, K. Urban, I. Vrejoiu, M. Alexe, and D. Hesse, Nat. Mater. **7**, 57 (2008).
[27]Y. L. Page, T. Siegrist, S. A. Sunshine, L. F. Schneemeyer, D. W. Murphy, S. M. Zahurak, J. V. Waszczak, W. R. Mckinnon, J. M. Tarascon, G. W. Hull, and L. H. Greene, Phys. Rev. B **36**, 3617 (1987).
[28]S. C. Abrahams, S. K. Kurtz, and P. B. Jamieson, Phys. Rev. **172**, 551 (1968).
[29]H. Chen, J. Callaway, and P. K. Misra, Phys. Rev. B **38**, 195 (1988).
[30]M. Magnuson, T. Schmitt, V. N. Strocov, J. Schlappa, A. S. Kalabukhov, and L.-C. Duda, Sci. Rep. **4**, 7017 (2014).
[31]N. Pavlenko and T. Kopp, Phys. Rev. B **72**, 174516 (2005).
[32]N. Pavlenko and T. Kopp, Phys. Rev. Lett. **97**, 187001 (2006).